Influence of synthesis conditions on growth of Ni-doped chrysotile

Influence of synthesis conditions on growth of Ni-doped chrysotile

Abstract

Ni-doped chrysotile fibers were synthesized in hydrothermal conditions at 300–350 °C, 15–200 MPa, 160–312 h treatment times and pH 5–10. The starting materials and run products were characterized by X-ray powder diffraction (XRPD) and by scanning and transmission electron microscopy, both with annexed energy-dispersive spectrometry (SEM/EDS and TEM/EDS, respectively). The growth of Ni-doped chrysotile fibers depends greatly on the starting materials: they are observed as run products only starting from synthetic Ni-doped forsterite. When oxides are used as starting phases, even in the same hydrothermal conditions, the growth of Ni-doped talc is observed. As regards the morphology of synthesized chrysotile fibers, under the conditions of the present work, cone-in-cone crystals were prevalent, but other morphologies were also detected, all showing well-defined crystallinity, as revealed by electron diffraction patterns of selected areas (SAED). Fibers with cylindrical shape showed outer diameters ranging from 37 to 52 nm and a central hollow (empty core) ranging from 6 to 10 nm. The average concentrations of nickel oxide in chrysotile fibers varied from 4 to 11 (wt%). Further characterization by differential scanning calorimetry (DSC)/thermogravimetric (TG) and by μ-Raman spectroscopy allowed to study the effect of Ni doping on the chemical/physical characteristics of the chrysotile fibers.

1. Introduction

Research on nanostructure materials are currently addressed to synthesis and characterization of new types of micro- and mesoporous silicates, because of their considerable potential applications in many areas such as molecular sieves, gas sensors and catalyst agents [1], [2] and [3]. Fibrils of chrysotile are considered as porous silicates and also nanotubes on the basis of their morphology and diameter [4] and [5]. Chrysotile with ideal chemical formula $Mg_3Si_2O_5(OH)_4$ is a 1:1 phyllosilicate belonging to the serpentine group [6]. Structurally, it is built up of sheets of linked tetrahedral silica-oxygen groups [SiO_4] (T) joined to brucite-type [$Mg(OH)_2$] octahedral sheets (O) [7]. In the chrysotile structure, the TO layers are curved to form cylindrical and/or spiralized fibers having generally an empty central tube (core). Their ideal radius is 88 Å as calculated by Wicks and Whittaker [8]. Based on the mismatch in the lateral dimensions of the two T–O sheets and on the elasticity of the serpentine layers, Perbost et al. [9] estimated that nickel 1:1 phyllosilicate particles should have a radius of curvature of about 90 Å.

Although chrysotile fibers have good technological properties, when breathed in high doses by humans or animals, they may cause several respiratory diseases (e.g. [10], [11], [12] and [13]) and their use is therefore limited or forbidden in several countries. However, during the last years pure and doped chrysotile [14] have been synthesized by several researchers, proposing their use as semiconducting nanowires or as replacements for carbon nanotubes [15], [16], [17], [18], [19] and [20]. The fibers are called nanotubes when of nanometric diameter (e.g. [21], [22] and [23]).

So far chrysotile fibers have been doped only with differing amounts of iron [24] and [25], nickel [26] and [4], and titanium [27]. Certainly, it is very important that toxicity tests of these synthetic doped chrysotile fibers as well as of those of stoichiometric composition [28] should be carefully carried out before they are used in industry, to ensure that they cannot produce risks for human health. To this aim it is very important take in account that (i) the presence of impurities (i.e., Fe, Ni, Ti) to ideal chemical composition in chrysotile fibers, even in small amounts, affects their chemical/physical properties and size [24], [25], [26], [27] and [29], (ii) according to in vitro studies on biological system-mineral interactions, both characteristics (impurities and size) are considered to be responsible for the pathological effects [30]. Therefore, following all the above reasons, different kinds of doped chrysotile would be synthesized and in detail characterized. Korytkova et al. [26] grew hydrothermally Ni-doped chrysotile nanotubes (Mg, Ni)3Si2O5(OH)4 using NiO and MgO as starting mixture, at relatively high temperature and pressure (400 °C, 70 MPa) and observed that: (i) at lower temperatures, only small amounts of short tubes, mixed with mostly small thin platelets, were produced, (ii) at higher temperatures, Ni-doped talc and Ni-doped olivine were synthesized. However, when a mixture of NiSiO3 and MgO was used, in the same temperature and pressure conditions (400 °C, 70 MPa), Ni3Si2O5(OH)4 nanotubes were obtained. According to McDonald et al. [4] Ni3Si2O5(OH)4 nanotubes grew as unique phase when nickel chloride, silicic acid and sodium hydroxide were used as starting mixture at relatively low temperature and pressure (250 °C, 10 MPa). The outer diameters of the resulting tubes ranged from 25 to 30 nm, with an inner diameter of 10 nm, very close to that of natural chrysotile fibers, which have outer and inner diameters of 22–27 and 7–10 nm, respectively [22], [23] and [31]. These values for Ni3Si2O5(OH)4 tubes were larger than those reported by Korytkova et al. [26], who reported outer and inner diameters of 10–30 and 2–5 nm respectively for nanotubes obtained at 400 °C and 70 MPa. According to the above authors, Ni substitution for magnesium reduces size of the fibers and enhances their thermal stability. The length of Ni-doped chrysotile nanotubes obtained in previous works/experiments ranged between 200 nm [4] and 30 000 nm [26], whereas natural chrysotile fibers showed lengths ranging from few nanometers to several centimeters [22], [23] and [31]. Taking into account literature reports, the formation and size of Ni-doped chrysotile depend on starting materials, growth conditions and dopant amount.

As regards the morphology of synthetic chrysotile, Foresti et al. [25] demonstrated that increasing amounts of Fe in the chrysotile lattice may lead to changes from fibrous to flat morphology [25]. However, other authors emphasized the roles played by starting materials and experimental conditions on the various Fe–Ti-doped chrysotile morphologies obtained [24] and [27].

Natural and synthetic chrysotile fibers show a wide variety of shapes: hollowed cylinder, non-hollowed cylinder, tube-in-tube, conically wrapped, spiralized (helical) and cone-in-cone fibers [14], [31] and [32]. As regards Ni-doped chrysotile, not all these morphologies have been obtained in previous studies [26] and [4]. The different morphological varieties may have a specific stability field (P–T), but they co-exist in the same growth conditions (T, P, time, pH, doping amount), so that the question on which synthesis variable controls the type of chrysotile morphology remains open.

In the context described here, and in the light of the potential of these fiber application to advanced technologies, the present work aimed at determining the influence of various synthesis variables

(conditions, amount of Ni-doping, starting materials) on the morphology, size and some chemical/physical features of grown Ni-doped chrysotile nanotubes.

2. Experimental

2.1. Characterization

Both the starting materials and the experimental run products were characterized by powder X-ray diffraction (XRPD), scanning and transmission electron microscopy (SEM and TEM) and energy-dispersive spectrometry (EDS), thermogravimetric (TG) and differential scanning calorimetry (DSC) and micro-Raman spectroscopy. XRPD patterns were obtained on a Philips PW 1730 diffractometer, operating at 40 kV and 20 mA, with Cu Kα radiation. Secondary electron SEM imaging was performed on a FEI Quanta 200 equipped with a field emission gun (FEG). Transmission electron microscopy (TEM Philips CM12, working at 120 kV with a LaB6 filament) with a double tilt holder was used to perform morphological observations and to obtain structural data by selected area electron diffraction (SAED); an EDS EDAX system with Si/(Li) annexed detector allowed to obtain analytical electron microanalyses (AEM). AEM data were processed with the SUPQ software PV9800 system, with default K factors to obtain normalized quantitative data. For TEM investigations, a fragment of the run product was gently disaggregated in isopropyl alcohol using an agate and pestle mortar and then sonicated; two drops of the obtained suspension were deposited on a gold mesh grid coated with 200 Å carbon film. Thermogravimetric and differential scanning calorimetry (TG–DSC) was performed in an alumina crucible under a constant nitrogen flow of 30 cm3 min−1 with a Netzsch STA 449 C Jupiter in 25–1000 °C temperature range, and a heating rate of 10 °C/min.

The micro-Raman equipment used during this work was a Jobin Yvon HR800 LabRam μ-spectrometer equipped with an Olympus BX41 microscope, an HeNe 20 mW laser working at 632.8 nm, and a CCD air-cooled detector. The instrument was correctly calibrated by checking the position and intensity of the Si band at ±520.6 cm−1 before every run. Spectra were recorded in the spectral region from 1200 to 200 cm−1, corresponding to lattice vibrational modes and identified by Rinaudo et al. (2003) [33] as characteristic for distinguishing serpentine minerals. In order to balance the signal against noise, the spectra were recorded in 100 cycles of 10 s each, at resolution of 1 cm−1. The spectra were then processed by ORIGIN vers. 6.0 software.

2.2. Starting materials

The starting materials for the experiments were: synthetic Ni-doped forsterite; SiO_2 granular quartz (Carlo Erba reagent, code No. 364011) converted into cristobalite by heating at 1400 °C; NiO nickel oxide (Sigma–Aldrich reagent, code No. 1313-99-1). Ni-doped forsterite was synthesized according to the technique described by Bloise et al. [34]. Only crystals that showed a uniform and light-green color, being free from impurities visible under a stereo binocular microscope (20×), were used in these experiments. No other phases except forsterite were detected by X-ray powder diffraction (XRPD) and transmission electron microscopy (TEM).

The average amount of NiO wt%, in forsterite, calculated on 23 analytical electron microscopy (AEM-TEM) semi-quantitative analyses, was 13%, this value matching the following composition: (Mg1.70Ni0.26)Si1.02O4.

2.3. Treatment of starting materials

Two different types of apparatus were used during this work: a vertical furnace with a Super Kanthal heating element (0–1700 °C) and an externally heated pressure vessel (Kanthal heating wire 0–1000 °C). In the former, the temperature was controlled by PtRh–PtRh thermocouples (precision ±4 °C) and continuously monitored; the latter had two chromel–alumel thermocouples (precision ±2.5 °C, calibrated on the freezing point of NaCl, i.e., 800.5 °C) placed near the hottest portion of the device. Pressure inside the external heated vessel was supplied through a hydrostatic circuit and continuously monitored by a Nova Swiss transducer system (accuracy ±5 bar).

2.4. Hydrothermal synthesis of Ni-doped chrysotile

Selected Ni-doped forsterite crystals were cleaned by sonication in hot water for 30 min, crushed in an agate mortar and sieved, producing fraction grains with sizes of less than 0.177 mm to use for experiments. Cristobalite (SiO2) and nickel oxide (NiO), weighed according to an ideal stoichiometric formula Ni3Si2O5(OH)4, were mixed in an agate mortar.

About 30 mg of powdered mixture, added to bidistilled water (14% in weight), were sealed in a platinum capsule (0.11 cm3 in volume) with an arc-welder. Synthesis was carried out in neutral conditions, basic (NaOH was added to reach pH 10) and acid (HCl was added to obtain pH 5) starting solutions. The capsules were weighed before and after runs, to check weight variations. Several runs of hydrothermal synthesis were carried out in externally heated pressure vessels in the following conditions: temperature 300–350 °C; pressure 15–200 MPa; time 160–312 h. The experimental conditions are listed in Table 1. Lastly, the capsules were rapidly quenched in water at an estimated cooling rate of about 300 °C/min.

Table 1.

Run	**Starting mixture**	***T* (°C)**	***P* (MPa)**	**pH**	***t* (h)**	**XRPD**	**SEM–TEM–EDS**
Ni1	Ni-doped forsterite	350	80	7	160	Fo, Ctl, Bt	Ni–Fo, Ni–Ctl, Ni–Bt
Ni4	Idem	350	50	5	240	Fo, Ctl, Bt	Ni–Fo, Ni–Ctl, Ni–Bt
Ni3	Idem	300	100	5	160	Fo, Ctl, Bt	Ni–Fo, Ni–Ctl, Ni–Bt
Ni5	Idem	300	100	7	160	Ctl, Fo, Bt	Ni–Ctl, Ni–Fo, Ni–Bt
Ni6	Idem	350	15	7	240	Ctl, Bt, Ni	Ni–Ctl, Ni–Bt, Ni

Run	Starting mixture	*T* (°C)	*P* (MPa)	pH	*t* (h)	XRPD	SEM–TEM–EDS
Foni3	Oxides	300	15	10	312	Qtz, NiO	NiO, Qtz
Foni7	Idem	300	100	10	160	Qtz, NiO, Tlc	NiO, Qtz, Ni–Tlc
Foni5	Idem	350	50	10	240	Qtz, NiO, Tlc	NiO, Qtz, Ni–Tlc
Foni4	Idem	350	200	10	240	Qtz, NiO, Tlc	Ni–Tlc, NiO, Qtz
N7	Idem	300	100	7	160	Tlc, NiO, Qtz	Ni–Tlc, NiO, Qtz
Ni13	Idem	300	100	5	160	Tlc, NiO	Ni–Tlc, NiO
N10	Idem	350	15	7	240	Tlc, NiO	Ni–Tlc, NiO

Experimental conditions and product list of synthesis for each synthesis in order of decreasing abundance, as detected by XRPD, SEM and TEM with EDS. Ctl = chrysotile; Bt = brucite; Fo = forsterite; Tlc = talc; Ni–Ctl = Ni-doped chrysotile; Ni–Bt = Ni-doped brucite; Ni–Fo = Ni-doped forsterite; Ni–Tlc = Ni-doped talc; Qtz = quartz; Ni = metallic nickel; NiO = nickel oxide.

3. Results and discussion

3.1. Characterization of Ni-doped chrysotile fibers

The experimental conditions and results of all experimental runs are listed in Table 1. At 350 °C, 80 MPa and 160 h (run Ni1), small amounts of Ni-doped chrysotile were detected by XRPD analyses. The crystallized fibers, few micrometers in length (Fig. 1a), were characterized by rather poor crystallinity, as confirmed by TEM observations. Higher pressure, lower temperature and the same synthesis time (run Ni3), produced more abundant and longer Ni-doped chrysotile fibers (Fig. 1b). Ni-doped forsterite still appeared in both runs, their surfaces being covered by small fibers of Ni-doped chrysotile (Fig. 1b). Matching the observations of Bostjan and Suvorov [35], acid conditions of the starting solution did not improve the reaction toward more abundant growth of Ni-doped chrysotile and a greater length of fibers. Lastly, at 350 °C and 15 MPa, with reaction times of 240 h (run Ni6), Ni-doped forsterite was totally altered and Ni-doped chrysotile clearly prevailed over Ni-doped brucite and small amounts of metallic nickel (Fig. 2). In this last run (Ni6), chrysotile crystallized as long bundles of fibers, several micrometers long, some of them even reaching 30 μm (Fig. 3a).

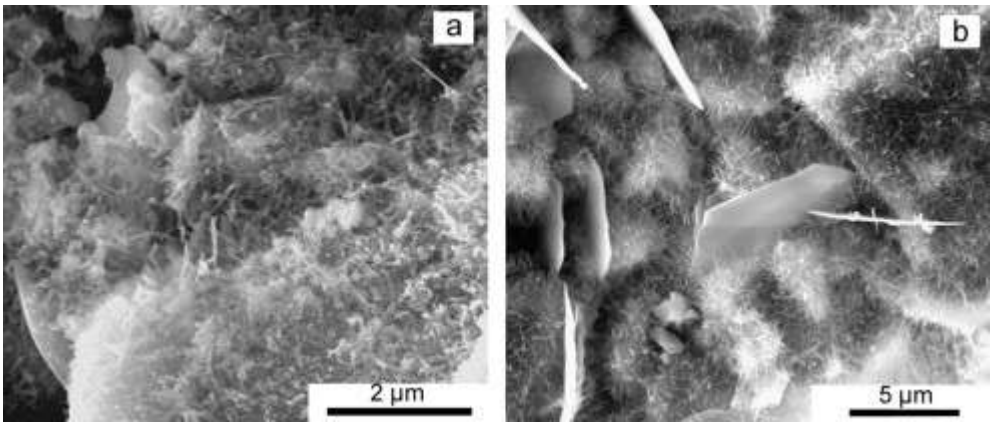

Fig. 1.

Secondary electron SEM images of various run products: (a) Ni-doped chrysotile, run Ni1 (350 °C, 80 MPa, 160 h, pH 7); (b) Ni-doped chrysotile, also covering Ni-doped forsterite relics (right upper corner) and polygonal platelets of Ni-doped brucite, run Ni3 (300 °C, 100 MPa, 160 h, pH 5).

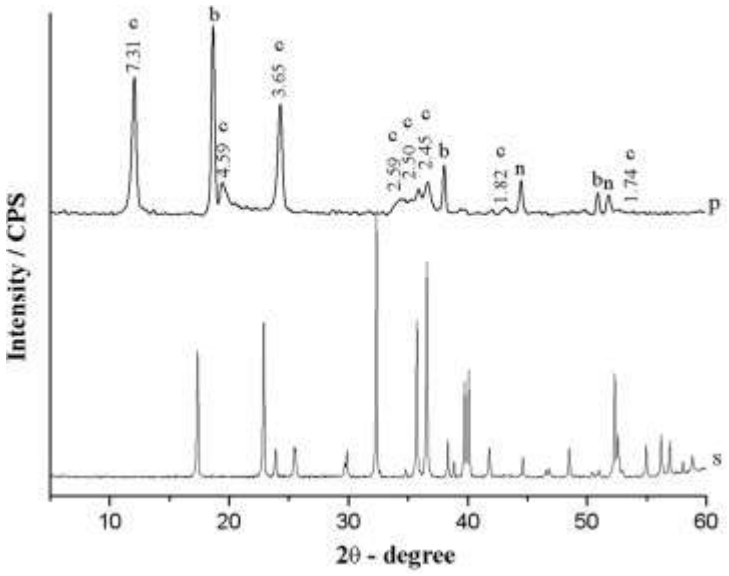

Fig. 2.

XRPD patterns: lower part (s), starting material, consisting of Ni-doped forsterite (Ni–Mg2SiO4) (JCPDS 34-0189); upper part (p) reaction product after 240 h in hydrothermal conditions of 350 °C, 15 MPa and pH 7 (run Ni6); c = clinochrysotile (JCPDS 10-0380) with relative spacings in Å, b = brucite (JCPDS 44-1482), n = Ni (JCPDS 04–0850).

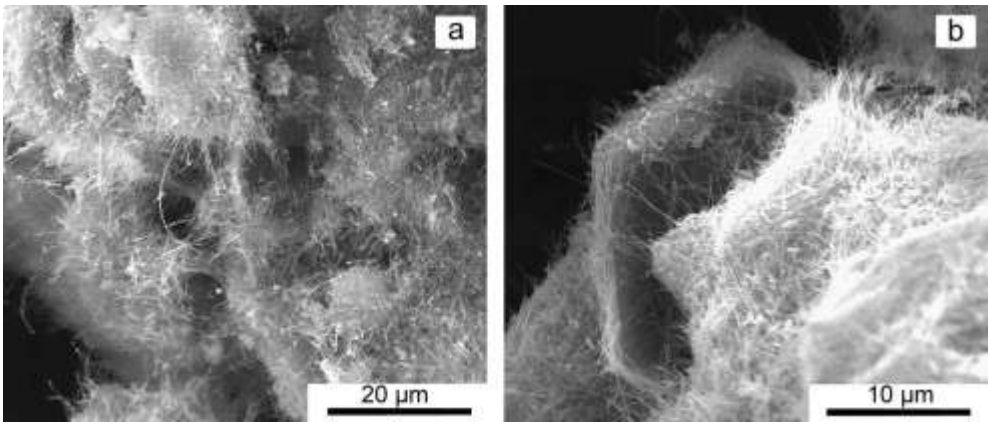

Fig. 3.

Secondary electron SEM images of (a) Ni-doped chrysotile; (b) hexagonal platelets of Ni-doped brucite wrapped by Ni-doped chrysotile (run Ni6: 350 °C, 15 MPa, 240 h, pH 7).

Ni-doped brucite crystals occurred in all runs in amounts lower than the other products. The intense peaks ascribed to brucite in the XRPD patterns (Fig. 2) are the consequence of flattened morphology, producing preferential orientation of the crystals in the analyzed powder. In some cases, Ni-doped chrysotile fibers wrapped platelets of Ni-doped brucite (Fig. 3b), with fibers approximately 18 µm in diameter and 1 µm thick. On the whole, the best conditions for more abundant and greater lengthening of fibers were 350 °C, 15 MPa, 240 h and pH 7 (run Ni6). Pressure and temperature were respectively higher and lower than those reported by Korytkova et al. [26] for (Mg,Ni)3Si2O5(OH)4 nanotubes, but similar to those reported by McDonald et al. [4] for Ni3Si2O5(OH)4 nanotube synthesis. However according to our opinion, in order to obtain Ni-doped chrysotile nanotubes, the characteristics of the starting materials are more crucial that synthesis conditions. In fact, no chrysotile was obtained in runs in which oxides were used as starting mixture. In four out of seven runs, XRPD revealed the formation of talc and quartz, in addition to the starting NiO (Table 1, second part). Also when oxides were hydrothermally treated in the conditions of run Ni6 (350 °C, 15 MPa, 240 h, pH 7), Ni-doped chrysotile did not form, but Ni-doped talc was the main product (run N10, Table 1). In all runs, Ni-doped talc crystallized in thin wavy lamellar sheets, micrometric in size, from about 1 to 10 µm in width.

TEM observations of single fibers showed cylinder, cone-in-cone, spiral and cylinder-in-cylinder morphologies (Fig. 4 and Fig. 5), all characterized by high crystallinity as confirmed by SAED patterns. No fibers with diameters greater than 100 nm, which generally show polygonal habit as reported in the literature [23], [36] and [37], were obtained. The central core of all kinds of fibers always runs empty longitudinally along the fibers, without interruptions. In some cases, cylindrical fibers (Fig. 4 and Fig. 5a) show flared extremities (Fig. 5a), but the diameter of the internal core always remains constant along the fiber length. Fig. 4 and Fig. 5c show cone-in-cone Ni-doped chrysotile fibers, arranged in a detritus-like discharge. The SAED patterns (Fig. 5d) show the typical cone-in-cone split of the diffraction spots: the latter

do not lie in a straight line, as in a cylindrical crystal lattice, but on two lines, intersecting at an angle which depends on the cone angle (ø ≅ 16°). As a consequence, the split spots are not equidistant from the central spot, as shown in detail by Yada and Iishi [32]. In all runs, cone-in-cone morphology was more abundant, almost double quantity, than the cylindrical type (Fig. 6a). Ni-doped chrysotile fibers also showed spiral morphology (Fig. 4b), as illustrated in detail by Amelinckx et al. [31]; this shape is a precursor morphology leading to the conical one [32].

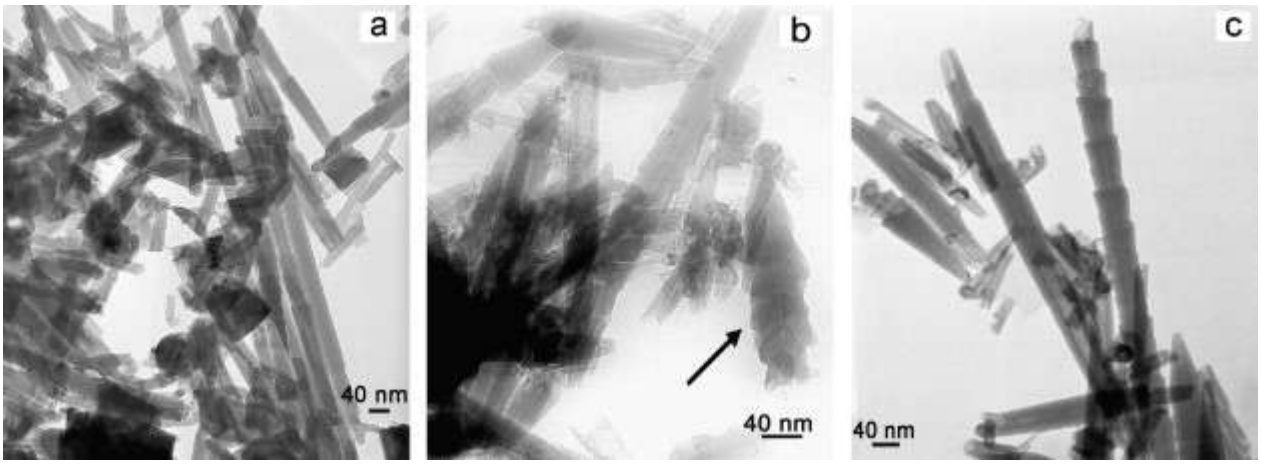

Fig. 4.

TEM micrographs of Ni-doped chrysotile obtained at various hydrothermal conditions: (a) run Ni1 (350 °C, 80 MPa, 160 h, pH 7); (b) run Ni3 (300 °C, 100 MPa, 160 h, pH 5), spiral morphology is indicated by arrow; (c) run Ni5 (300 °C, 100 MPa, 160 h, pH 7).

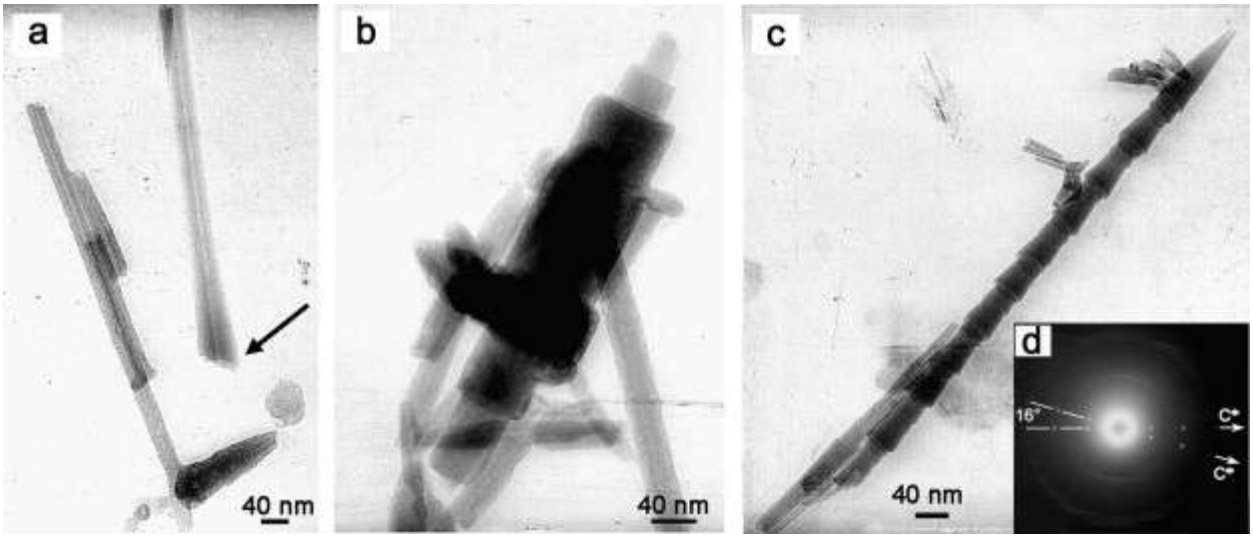

Fig. 5.

TEM micrographs of different morphologies of Ni-doped chrysotile fibers obtained at 350 °C, 15 MPa, 240 h, pH 7 (run Ni6): (a) cylinder: arrow indicates flared extremity; (b) cylinder-in-cylinder; (c) cone-in-cone; (d) electron diffraction pattern of conical fiber in 0kl plane with cone angle ø ≅ 16°.

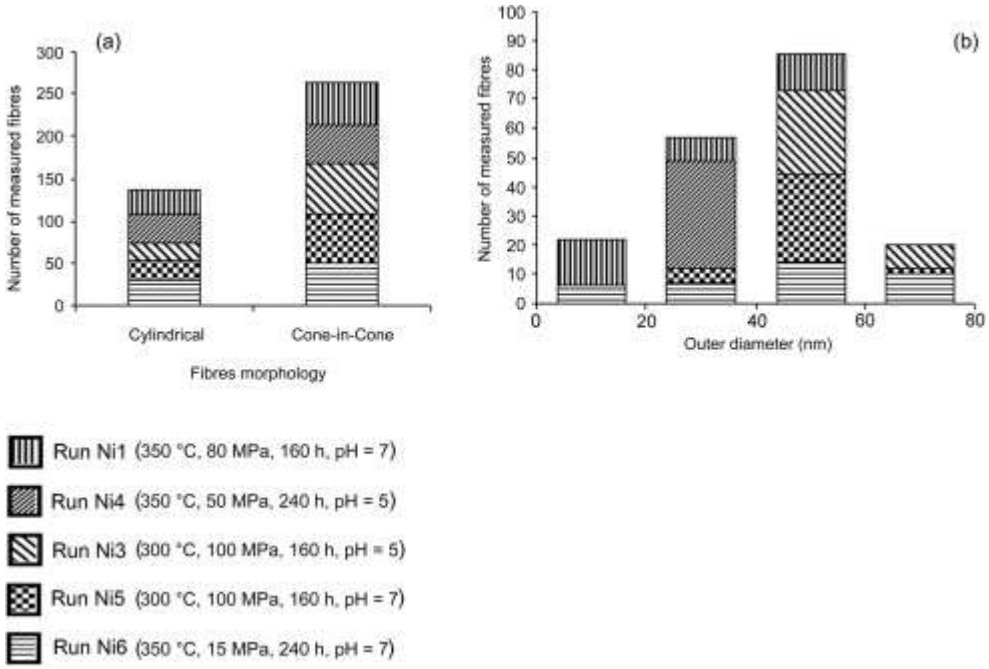

Fig. 6.

Histograms of Ni-doped chrysotile nanotubes from various runs: (a) fiber morphology; (b) outer diameter.

Probably owing to low Ni dopant amount, pressure and high reaction time (15 MPa, 240 h), only in run Ni6 some fibers were concentrically and telescopically arranged [24] and [35] (Fig. 5b).

Fibers with cylindrical shape have outer tube diameters varying from 37 to 52 nm, and inner core diameters ranging from 6 to 10 nm (Table 2); according to definition used by several authors [5], [35] and [38], with this kind of morphology and diameter, these fibers can properly be called nanotubes. The inner diameter values are greater than those reported by Korytkova et al. [26], but are closer to those of natural fibers [22], [23] and [39] and to those reported by McDonald et al. [4], and they also very well match the dimensions estimated by Perbost et al. [9].

Table 2.

Run	Length (μm)	Diameter (nm)		Outer/inner ratio	NiO (wt%)
		Outer	Inner		
Ni6	15	45	9	5.0	4.71
Ni3	1.2	52	9	6.0	11.44
Ni5	2.5	45	10	4.5	11.60
Ni1	1.0	40	9	4.2	11.78
Ni4	0.8	37	6	6.0	11.85

Morphological and chemical characteristics of Ni-doped chrysotile fibers (with tube morphology) from all runs (averaged values from several measures).

The outer diameters of the fibers crystallized in this work were greater than those of natural fibers [22], [23] and [39] and those synthesized by McDonald et al. [4] and Korytkova et al. [26]. The differences are certainly due to different hydrothermal treatment conditions and type of starting materials [4] and [26]. An acid starting solution yields fibers with constant outer/inner diameter ratios (Table 2) and the cylindrical fibers obtained in acid conditions (runs Ni3, Ni4) mostly show constant diameters (Fig. 7b). In particular, in run Ni3 (300 °C, 100 MPa, 160 h, pH 5) the outer diameters fell into two frequency classes (Fig. 6b) ranging from 40 to 80 nm. Instead, the fibers from run 4 (350 °C, 50 MPa, 240 h, pH 5) showed a nearly constant outer diameter, falling in only one frequency class, ranging from 20 to 40 nm (Fig. 6b). Conversely, in runs Ni1, Ni5 and Ni6, in a neutral environment (pH 7) the fibers exhibited greater differences in diameters (Fig. 6b), the widest being for run Ni6, corresponding to longest run time (240 h). Fiber lengths in all runs ranged from 0.8 to 15 μm; on the whole, with neutral pH values, the length increased with increasing reaction times.

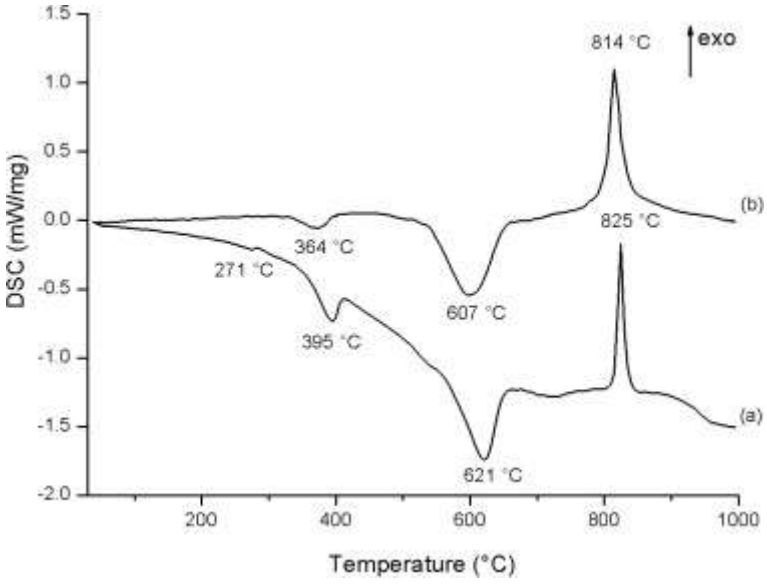

Fig. 7.

DSC curves of synthetic chrysotile fibers: (a) doped with 4.7 wt% of NiO (run Ni6); (b) doped with 11.8 wt% of NiO (run Ni4).

As regards chemical composition, AEM semi-quantitative analyses from 60 single fibers from all runs always show that Ni is present. The average amount of NiO wt% in the fibers didn't appear to cover a continuous range but rather was barred to two different amounts, about 4% and 11% (Table 2), therefore the representative chemical formulae are: $(Mg_{2.8}Ni_{0.2})Si_2O_5(OH)_4$–$(Mg_{0.6}Ni_{0.4})Si_2O_5(OH)_4$. Variations in Ni content substituting for Mg may be attributed to differing experimental conditions of synthesis (Table 1 and Table 2). Although only two orders of dopant amounts were detected in the fibers (about 4 and 11 wt% of NiO), an inverse correlation between Ni content and fiber length was detected (Table 2), in accordance with the results of Korytkova et al. [26].

In the same hydrothermal synthesis conditions (runs Ni3, Ni5), variations in pH values, from neutral (run Ni5) to acid (run Ni3), determined the decreasing of fiber lengths and Ni content and the enhanced of their diameter (Table 2). These results prove the sensitivity of Ni-doped chrysotile to changes in pH.

From the morphological and compositional points of view, all single fibers with cylinder-in-cylinder shape, detected only in run Ni6, had lower NiO content (NiO < 4.0 wt%) with respect to both cylinder and cone-in-cone crystals, which had an average value of 5.4 wt%. However, no correlation between Ni substitution for Mg and cylinder or cone-in-cone morphology was observed, their NiO content being nearly similar.

Fig. 7 compares the DCS curves of chrysotile with 4.7 (run Ni6) and 11.8 wt% of NiO (run Ni4) in the temperature range 30–1000 °C. These curves have a similar trend, and differ only in exo–endothermic

effect. As a matter of fact, the endothermic peaks at 395 °C and 621 °C (Fig. 7a), assigned to dehydroxylation respectively of Ni-doped brucite and Ni-doped chrysotile (run Ni6), were shifted to 364 °C and 607 °C (Fig. 7b) in the sample with higher Ni content (run Ni4). This means that an increase in Ni amount in chrysotile fiber (from 4.7 to 11.8 wt%) corresponds to a significant decrease in the decomposition peak temperature.

The anhydrous material remaining after Ni-doped chrysotile dehydroxilation recrystallized to forsterite, producing a sharp exothermic peaks at 825 °C and 814 °C [24], [25], [40] and [41] for runs Ni6 and Ni4, respectively.

Considering that the analyzed fibers (runs Ni4, Ni6) are similar in size (Table 2), the decrease in the temperature of dehydroxylation and recrystallization may be due to the increased Ni content in the chrysotile fibers.

In run Ni6 we also observe a weak exo-endothermic effect at 271 °C (Fig. 7a), due to the oxidation–reduction of Ni (Table 1). The TG curves for both runs showed continuous weight loss (about 13%), due to decomposition of Ni-doped brucite and Ni-doped chrysotile [40] and [41]. These data match the theoretical and experimental values from the literature on mass loss observed in natural and synthetic chrysotile fibers [24], [25], [40] and [41].

The sample from run Ni6, in which chrysotile was detected as the main phase, was also characterized by micro-Raman spectroscopy. A Raman spectrum is shown in Fig. 8 where, except for the band ascribed to brucite [42], well-defined bands produced by chrysotile are detected. Nevertheless, when the spectrum in Fig. 8 is compared with the Raman spectrum from stoichiometric synthetic chrysotile [43], shifts in some vibrational modes can be identified. The vibrational modes at 624 cm−1 in Raman spectra from stoichiometric chrysotile and produced by Mg–OH translations are now shifted toward lower wave-numbers, 620 cm−1; the bands at 469 and 436 cm−1 in the stoichiometric chrysotile – ascribed to vibrational translation of Mg–OH/bending modes of the SiO_4 tetrahedra and to Mg–OH translation respectively - are not detected in Ni-doped chrysotile. Also, the Raman bands produced by the vibrational modes of the SiO_4 tetrahedra are affected: the bands at 690 and 388 cm−1, ascribed to symmetric stretching modes (vs) of Si–Ob–Si linkages and to bending modes v5(e)– of SiO_4 tetrahedra respectively, plot at 694 and 392 cm−1 in stoichiometric synthetic chrysotile [43]. Among the bending modes of SiO_4 tetrahedra, detected at 348, 321 and 305 cm−1 in stoichiometric chrysotile, only the band at 348 cm−1 appears in run Ni6, whereas the bands at 321 and 305 cm−1 are not detected here. Instead, the band at 230 cm−1 (vibrations of O–H–O groups) does not show any significant shift.

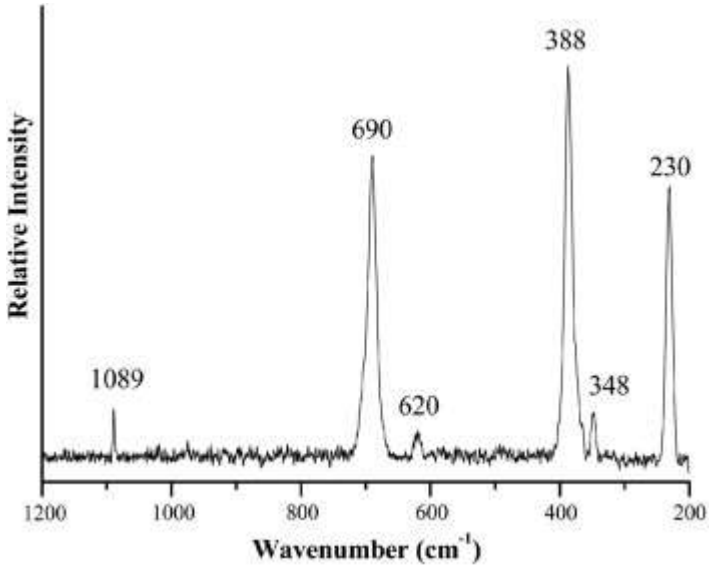

Fig. 8.

Raman spectrum of synthetic chrysotile doped with 4.71 wt% NiO (run Ni6). Band at 1089 cm−1 is ascribed to brucite.

The observed shifts toward lower frequencies may be due to the high concentration of Ni in the crystallized chrysotile or to the particular morphology of the crystals, that is, to the cone-in-cone growth shown in Fig. 4 and Fig. 5.

4. Conclusions

Chrysotile nanotubes doped with Ni were synthesized in hydrothermal conditions. Their growth seems to be closely related to the starting materials used, Ni-doped forsterite or oxides. In fact, Ni-doped chrysotile fibers were only obtained in runs when Ni-doped forsterite was used as starting material; when oxides were used, Ni-doped talc was obtained. The abundance of Ni-doped chrysotile nanotubes and their length depend on experimental conditions: the best conditions for more abundance and greater lengthening of fibers are 350 °C, 15 MPa and pH 7, with reaction times of 240 h. Variations in Ni content, substituting Mg in fibers composition, may be attributed to the differing experimental conditions in which the fibers are grown.

The relationships between experimental conditions (temperature, pressure, time, pH, Ni content) and fiber size and morphology are complex. However, in the case of Ni-doped chrysotile fibers, we observed that: (i) the same fiber diameters require acid pH, but this condition produces a decrease in their lengthening and abundance; (ii) with neutral pH, the increase of the reaction time enhances fiber length; (iii) the increase of Ni content in the nanotubes produces a decrease in their length. From the morphological point of view, in all runs the cone-in-cone morphology of Ni-doped chrysotile was more abundant than the cylindrical one. Ni amounts in cylinder, spiral and cone-in-cone morphologies were constant in all runs, whereas fibers with

cylinder-in-cylinder shape showed increasingly lower Ni content with respect to the other morphologies detected.

The decrease in dehydroxylation and recrystallization temperature with increasing Ni content in chrysotile fibers may be due to the different interlayer bond strength established, whereas the analyzed fibers are similar in size.

Deep knowledge of the effects of synthesis variables and the chemical–physical characteristics of Ni-doped chrysotile may increase its potential for new applications.

Synthesis of chrysotile fibers doped with different metal in various doses and their detailed characterization can be particular useful for in vitro test to improve the comprehension of the correlation between metal content of asbestos fibers and health problem.

References

[1]

in: G. Ferraris, S. Merlino (Eds.), Micro and Mesoporous Mineral Phases, Rev. Mineral. Geochem., vol. 57, Mineralogical Soc. America, Washington, DC (2005)

[2]

G. Ferraris, A. Bloise, M. Cadoni

Micropor. Mesopor. Mater., 107 (2008), p. 108

[3]

F.S. Xiao, Y. Han, X.J. Meng, Y. Yu, M. Yang, S. Wu

J. Am. Chem. Soc., 124 (2002), p. 888

[4]

A. McDonald, B. Scott, G. Villemure

Micropor. Mesopor. Mater., 120 (2009), p. 263

[5]

E.N. Korytkova, A.V. Maslov, L.N. Pivovarova, I.A. Drozdova, V.V. Gusarov

Glass Phys. Chem., 30 (2004), p. 51

[6]

W.A. Deer, R.A. Howie, J. Zussman

Rock-Forming Minerals Layered Silicates: Excluding Micas and Clay Minerals, vol. 3BThe Geological Society (2009)

[7]

F.J. Wicks, D.S. O'Hanley

Serpentine Minerals. Structures and Petrology, Rev. Mineral. Geochem., vol. 19

Mineralogical Soc. America, Washington, DC (1988)

[8]

F.J. Wicks, E.J.W. Whittaker

Can. Mineral., 13 (1975), p. 227

[9]

R. Perbost, M. Amouric, J. Olives

Clays Clay Miner., 51 (2003), p. 430

[10]

D. Bernstein, V. Castranova, K. Donaldson, B. Fubini, J. Hadley, T. Hesterberg, A. Kane, D. Lai, E.E. Mcconnell, H. Muhle, G. Oberdorster, S. Olin, D.B. Warheit

Inhalation Toxicol., 17 (2005), p. 497

[11]

M.E. Gunter, E. Belluso, A. Mottana

Amphiboles: Environmental and Health Concerns, in Rev. Mineral. Geochem., vol. 67Mineralogical Soc. America, Chantilly, VA (2007)

[12]

G.D. Guthrie, B.T. Mossman (Eds.), Merging the Geological and Biological Science an Integrated Approach to Mineral Induced Pulmonary Disease, in Health Effects of Mineral Dusts. Rev. Mineral. Geochem., vol. 28Mineralogical Soc. America, Chelsea, MI (1993)

[13]

C. Bergamini, R. Fato, G. Biagini, A. Pugnaloni, F. Giantomassi, E. Foresti, I. Lesci, N. Roveri, G. Lenaz

Cell. Mol. Biol., 52 (2007), p. 905

[14]

N. Roveri, G. Falini, E. Foresti, G. Fracasso, I.G. Lesci, P. Sabatino

J. Mater. Res., 21 (2006), p. 2711

[15]

M.S. Ivanova, Y.A. Kumzerov, V.V. Poborchii

Microporous Mater., 4 (1995), p. 319

[16]

H.M. Yates, W.R. Flavell, M.E. Pemble, N.P. Johnson, S.G. Romanov, C.M. Sotomayor-Torres

J. Cryst. Growth, 170 (1997), p. 611

[17]

S.G. Romanov, C.M. Sotomayor-Torres, H.M. Yates, M.E. Pemble, V. Butko, V.J. Tretijakov

J. Appl. Phys., 82 (1997), p. 380

[18]

K. Chernoutsan, V. Dneprovskii, S. Gavrilov, V. Gusev, E. Muljarov, S. Romanov, A. Syrnicov, O. Shaligina, E. Zhukov

Physica E, 15 (2002), p. 111

[19]

C. Metraux, B. Grobety, P. Ulmer

J. Mater. Res., 17 (2002), p. 1129

[20]

V.V. Poborchii, M.S. Ivanova, I.A. Salamatina

Superlattices Microstruct., 16 (1994), p. 133

[21]

K. Yada

Acta Crystallogr., 27 (1971), p. 659

[22]

E.J.W. Whittaker

Acta Crystallogr., 10 (1957), p. 149

[23]

A. Baronnet, E. Belluso

Mineral. Mag., 66 (2002), p. 709

[24]

A. Bloise, E. Belluso, E. Barrese, D. Miriello, C. Apollaro

Cryst. Res. Technol., 44 (2009), p. 590

[25]

E. Foresti Jr., M.F. Hochella, I.G. Lesci, A.S. Madden, N. Roveri, H. Xu

Adv. Funct. Mater., 15 (2005), p. 1009

[26]

E.N. Korytkova, A.V. Maslov, L.N. Pivovarova, Y.V. Polegotchenkova, V.F. Povinich, V.V. Gusarov

Inorg. Mater., 41 (2005), p. 743

[27]

A. Bloise, E. Barrese, C. Apollaro

N. Jb. Miner. Mh., 185 (2009), p. 297

[28]

E. Gazzano, E. Foresti, I.G. Lesci, M. Tomatis, C. Riganti, B. Fubini, N. Roveri, D. Ghigo

Toxicol. Appl. Pharmacol., 206 (2005), p. 356

[29]

G. Falini, E. Foresti, G. Lesci, N. Roveri

Chem. Commun., 14 (2002), p. 1512

[30]

B. Fubini, C. Otero-Ar´ean

Chem. Soc. Rev., 28 (1999), p. 373

[31]

S. Amelinckx, B. Devouard, A. Baronnet

Acta Crystallogr., Sect. A, 52 (1996), p. 850

[32]

K. Yada, K. Iishi

Am. Mineral., 62 (1977), p. 958

[33]

C. Rinaudo, D. Gastaldi, E. Belluso

Can. Mineral., 41 (2003), p. 883

[34]

A. Bloise, E. Barrese, C. Apollaro, D. Miriello

Cryst. Res. Technol., 44 (2009), p. 463

[35]

J. Bostjan, D. Suvorov

Nanotechnology, 17 (2006), p. 25

[36]

A. Baronnet, M. Mellini, B. Devouard

Phys. Chem. Miner., 21 (1994), p. 330

[37]

G. Papp

Annls. Hist. Nat. Mus. Natn. Hung., 82 (1990), p. 9

[38]

G.R. Patzke, F. Krumeich, R. Nesper

Angew. Chem., Int. Ed., 41 (2002), p. 2446

[39]

B.A. Cressey, E.J.W. Whittacher

Mineral. Mag., 57 (1993), p. 148

[40]

A. Cattaneo, A.F. Gualtieri, G. Artioli

Phys. Chem. Miner., 30 (2003), p. 177

[41]

F. Wypych, W.H. Schreiner, N. Mattoso, D.H. Mosca, R. Marangonia, C.A.S. Bento

J. Mater. Chem., 13 (2003), p. 304

[42]

F. Pascale, S. Tosoni, C. Zicovich-Wilson, P. Ugliengo, R. Orlando, R. Dovesi

Chem. Phys. Lett., 396 (2004), p. 308

[43]

E. Foresti, E. Fornero, I.G. Lesci, C. Rinaudo, T. Zuccheri, N. Roveri

J. Hazard Mater., 167 (2009), p. 1070